JBIC Journal of Biological Inorganic Chemistry (2020) 25:325–338
https://doi.org/10.1007/s00775-020-01764-5

ORIGINAL PAPER

Cytotoxicity and cell death induced by engineered nanostructures (quantum dots and nanoparticles) in human cell lines

Javed Ahmad[1,2] · Rizwan Wahab[1,2] · Maqsood A. Siddiqui[1,2] · Quaiser Saquib[1,2] · Abdulaziz A. Al-Khedhairy[1]

Received: 25 November 2019 / Accepted: 12 February 2020 / Published online: 2 March 2020

Abstract

In recent years, the industrial use of ZnO quantum dots (QDs) and nanoparticles (NPs) has risen and there is a high chance of these nanoparticles affecting human health. In this study, different sizes of ZnO-NPs (6–100 nm) were prepared and characterized. The generation of reactive oxygen species (ROS) and its involvement in apoptosis when HepG2 cells were exposed to QDs (6 nm) and NPs of different sizes (15–20, 50, and 100 nm) was also investigated. At a concentration of 25–200 µg/mL, NPs induced dose-dependent cytotoxicity in HepG2 cells. The engineered NPs increased oxidative stress in a dose- and size-dependent manner, as seen by an increase in ROS production, lipid peroxidation, and glutathione reduction. Furthermore, cell-cycle analysis of HepG2 cells treated with different sizes of NPs showed an increase in the apoptotic peak after a 24-h exposure period. Quantitative real-time PCR data showed that the mRNA levels of apoptotic marker genes such as p53, bax, and caspase-3 were upregulated, whereas bcl-2, an anti-apoptotic gene, was downregulated; therefore, apoptosis was mediated through the p53, bax, caspase-3, and bcl-2 pathways, suggesting a possible mechanism by which QDs and NPs of ZnO mediate their toxicity.

Graphic abstract

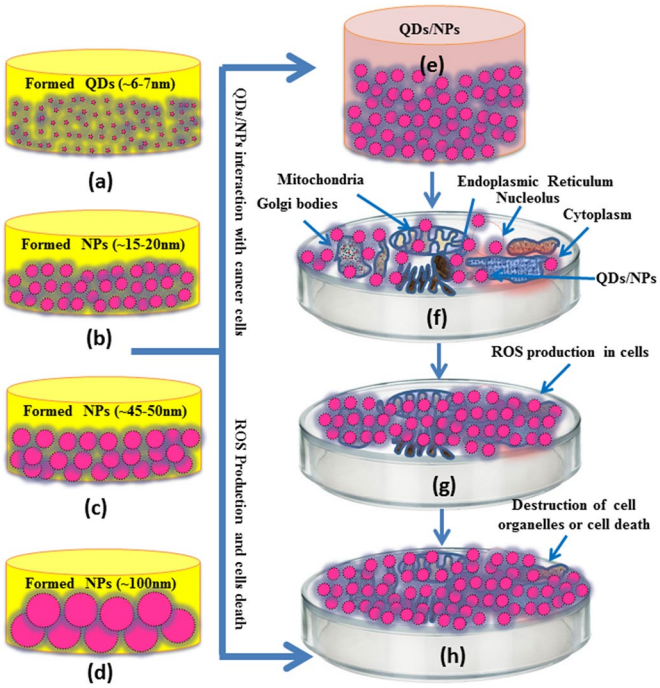

Keywords HepG2 cancer cells · MTT · Flow cytometry · ROS · QDs

Electronic supplementary material The online version of this article (https://doi.org/10.1007/s00775-020-01764-5) contains supplementary material, which is available to authorized users.

Extended author information available on the last page of the article

Introduction

The size of nanostructured materials is an important parameter in nanotechnology. Due to the small size of nanoparticles, their physicochemical properties such as volume, surface area, pore diameter, catalytic properties can change [1–5]. To date, various types of nanostructures in the form of quantum (QDs) [6], nanoparticles (NPs) [7], microparticles [8], thin films [9], and nanocomposites (NCs) have been created [10]. These fabricated structures are classified on the basis of their surface geometry such as zero, one, two, or three dimensional [11]. These structures are prepared by various chemical and physical methods, such as plasma-enhanced chemical vapor deposition [12], chemical vapor deposition [13], thermal evaporation [14], pulsed laser deposition [15], metal organic chemical vapor deposition [16], and cyclic feeding chemical vapor deposition [17]. Various physicochemical methods can also be used to prepare nanoparticles, such as template-assisted synthesis [18]; electrochemical [19], sol–gel [20], sonochemical [21], and surfactant-assisted growth methods [22]; hydrothermal synthesis [23]; and solvothermal [24], aqueous, and non-aqueous solution process [25]. The physical approaches are expensive as compared to the chemical methods, but provide nanomaterials in bulk [25]. Due to their small size and enhanced surface area, nanosized materials exhibit enormous fascinating properties, such as piezoelectric effect, high temperature tolerance, enhanced conductivity, and non-linear optical properties [26], which makes them excellent for a wide range of applications in the optoelectronic industry. These materials can be utilized in solar cells, dye-sensitized solar cells, fuel cells, hydrogen production, photocatalysis, adsorption, dye degradation, coatings, corrosion protectors, and semiconductor devices [25, 27–29].

Among numerous semiconductor metal oxides, zinc oxide (ZnO) is widely known for its versatile nature and can produce a series of nanostructures [30]. Zinc oxide has electronic properties, biocompatible nature, and can be used in various applications. However, there are limited reports on the use of different sized nanostructures, such as ZnO and TiO_2 NPs, their biological activity and efficacy against cancer cells. Few studies have evaluated their toxic effects against human blood cells or have evaluated their effect on the cellular and genetic material and ROS generation [31]. Previously, ZnO-NPs have been prepared by mechano-chemical reaction processes, where the size of the NPs was within 15–40 nm range, and the UV absorbance effects on NPs was checked [32]. The size-controlled ZnO-NPs were employed to examine the toxicity within different cells and their effect on the human immune system was studied [33]. The cytotoxicity was also measured with two spherical shaped zinc oxide NPs in terms of particle size, concentration, and time dependence in normal cells and cancer cell lines from different histological origins [34]. The ZnO particles were prepared in nano and micro-ranges for toxicity studies in human lung epithelial cells (L-132) and human monocytes (THP-1), which were chosen for their ability to clear foreign particles [35]. Three different sizes of ZnO-NPs (30 nm, 80–150 nm, and 2 µm) were used to check the cytotoxic and embryotoxic effects in flounder gill cells and zebrafish embryos [36]. The biological effects of ZnO-NPs were checked on SHSY5Y cells incubated for 24 h with various concentrations of NPs [37]. In another work, the nano and micro sized zinc oxide particles were utilized to check the cell viability, phagocytosis, and cytokine induction in human monocytes, THP-1 cells, which exhibit monocyte like properties and are linked with the adaptive and innate immune responses [38].

Here, we have described the preparation and characterization of different sized NPs. The study was designed to investigate the effect of NPs in liver cancer cells (HepG2) with different sized NPs, from 6 to 100 nm. HepG2 cells were used, because they are a well-established model system to study xenobiotic induced cell death. Different sized NPs were used to induce cell death/apoptosis in cancer cells. The MTT assay was used to check the % of viable and non-viable cells before and after interaction with nanomaterials, whereas apoptosis was measured via the flow cytometry. RT-PCR analysis of apoptotic gene p53, bax, caspase-3, and bcl-2 was also done.

Materials and methods

Synthesis of ZnO nanoparticles ranging from 6 to 100 nm was carried out at different conditions using different precursors. Four different kinds of particles were synthesized.

Synthesis of different sized zinc oxide nanoparticles

Quantum dots (ZnO-QDs) (Size ~ 6 ± 2 nm)

The ZnO-QDs were synthesized using analytical grade chemicals, purchased from Aldrich Chemical Co. Ltd. Zinc acetate dihydrate ($Zn(Ac)_2{\cdot}2H_2O$, 0.3 M), sodium hydroxide (NaOH, 0.3M) and aniline ($C_6H_5NH_2$, 20 mL) were mixed with 100 mL of methanol (MeOH) and stirred for 30 min. The inital pH of the solution was maintained at 6.87 using a pH meter (Cole Parmer, USA) and it increases up to 12.5 once the NaOH was incorporated. The stirred solution was refluxed in a glass pot at ~ 65 °C for 6 h. The organic impurities were removed from the solution by centrifugation (3000 rpm for 10 min). No precipitate was seen in the refluxing pot before 6 h. After refluxing was complete, a white

precipitate was obtained in the refluxing pot. The solution was dried in a petri dish and cooled at 25 °C [39].

Synthesis of ~ 15 ± 20-nm ZnO-NPs

Synthesis of ZnO-NPs, ranging from 15 to 20 nm, was done using $Zn(Ac)_2{\cdot}2H_2O$ and octadecylamine ($CH_3(CH_2)_{17}NH_2$). Briefly, 0.8 M $CH_3(CH_2)_{17}NH_2$ and 0.3 M $Zn(Ac)_2{\cdot}2H_2O$ were dissolved in 100 mL MeOH. The solution was stirred for 30 min on a hot plate equipped with a rotor. $Zn(Ac)_2{\cdot}2H_2O$ and octadecylamine were purchased from Aldrich Chemical Corporation. The pH of the solution was measured to be 12.3. After complete dissolution of the chemicals, the solution was transferred to a three-necked refluxing pot and refluxed at ~ 65 °C for 6 h. A white-colored precipitate was observed at the bottom of refluxing pot after 6 h. Solution temperature was monitored and controlled using a temperature controller. Thereafter, the white powdery precipitate was washed with MeOH several times. The NPs obtained were air dried at room temperature and their structural and chemical properties were characterized, as described previously [39].

Synthesis of 45 ± 5-nm ZnO-NPs

Bigger sized NPs were obtained by the reacting $Zn(AC)_2{\cdot}2H_2O$ and thiourea (NH_2CSNH_2) via solution process as previous [5, 20]. Briefly, 0.3 M $Zn(AC)_2{\cdot}2H_2O$ and 2 M NH_2CSNH_2 were dissolved in 100 mL deionized water and stirred for 30 min. The solution was then transferred to a glass pot and refluxed at 90 °C for 12 h. Before transferring the solution to the flask, the pH was measured at 12.6. After refluxing, the white aqueous solution was washed with MeOH several times to remove ionic impurities and then dried at 25 °C for further analysis. The dried powder was annealed in ambient air at 500 °C for 1 h at 5 °C/min. Thereafter, the morphological and chemical properties of NPs were characterized, as described previously [5, 20].

Synthesis of ~ 100-nm ZnO-NPs via the using solution method

The synthesis of ZnO-NPs (> 50 nm) was carried out using $Zn(AC)_2.2H_2O$ and p-xylene ($C_6H_4(CH_3)_2$), purchased from Aldrich Chemical Co. Ltd. Briefly, 0.3 M $Zn(Ac)_2.2H_2O$ and 20 mL $C_6H_4(CH_3)_2$ were mixed together in MeOH and stirred for 30 min. The pH of the solution was measured at 12.4. The stirred solution was transferred to the refluxing pot and refluxed at ~ 65 °C for 6 h followed by cooling at room temperature. The impurities, such as by-products of organic chemicals, were removed from the solution via centrifugation (3000 rpm for 5 min). The dried sample was annealed in ambient air at 700 °C for 1 h at 5 °C/min. Thereafter, the morphological and chemical properties of the sample were characterized [5, 20].

Characterization of different sized QDs and NPs prepared via solution process

The powders, with diverse sized particles, were morphologically and chemically characterized. Morphological evaluation of the white powder was made by field emission scanning electron microscopy (FESEM) and transmission electron microscopy (TEM). For FESEM, the white powders were uniformly sprayed on carbon tape and coated with a thin layer of osmium oxide (OsO_4) for 5 s. For TEM measurement, powder samples were sonicated in ethanol for 10 min. To this solution, copper grid was inserted for 2–3 s and dried at room temperature. The crystallinity and phase of the white powders were characterized with an X-ray powder diffractometer (XRD) with $Cu_{K\alpha}$ radiation ($\lambda = 1.54178$ Å) in the range of 20°–65° at 6°/min scanning speed.

Cell culture and their treatment of ZnO-NPs

Human liver HepG2 cells were purchased from ATCC, USA. Cells were cultured in DMEM/F-12 medium with 10% FBS and 100 U/mL penicillin–streptomycin in 5% CO_2 at 37 °C. The cells were harvested at 85% confluence using 0.25% trypsin and sub-cultured as required for the experiments. Cells were allowed to attach to the surface before treatment for 24 h. ZnO-QDs and NPs were suspended in culture medium and diluted to suitable concentrations. The dilutions of different sized NPs were then sonicated to avoid their agglomeration prior to their being applied to the cells.

MTT assay

Percent viability of HepG2 cells was assessed by exposing them to different concentrations of ZnO-NPs of various sizes, using the 3-(4,5-dimethylthiazol-2-yl)-2,5-diphenyltetrazolium bromide (MTT) assay, as described previously [40]. The assay evaluated cell viability by quantifying viable cells that reduced MTT to form a blue formazan product. In brief, 1×10^4 cells/well were incubated with 0, 1, 2, 5, 10, 25, 50, and 100 µg/mL QDs and NPs for 24 h. Subsequently, the medium in each well was exchanged with fresh medium, containing MTT at a final concentration of 10%, and incubated for 3 h at 37 °C for the purple color to develop. The formazan product so formed was dissolved in acidified isopropanol. The plate was centrifuged for 5 min at 2500 rpm for the QDs and NPs to settle at the bottom. Thereafter, 100 µL supernatant was taken from each well, transferred to fresh 96-well plate, and absorbance was quantified at 570 nm using a microplate reader (Synergy-HT,

BioTek). Percent viability of HepG2 cells was calculated using the formula,

$$\% \text{ Viability} = \text{mean absorbance of treated group} / \text{mean absorbance of control group} \times 100.$$

NRU assay

Neutral red uptake (NRU) assay was done as described by Borenfreund and Puerner (1984) [41], with some modifications [42]. In brief, 1×10^4 cells/well were seeded in 96-well plates, and incubated with 0, 1, 2, 5, 10, 25, 50, and 100 µg/mL QDs and NPs for 24 h. Thereafter, the supernatant was removed, the cells were washed with PBS, and incubated for 3 h in medium containing 50 µg/mL neutral red. The solution was removed promptly and the cells were washed with medium containing 0.5% formaldehyde and 1% calcium chloride. Subsequently, the cells were incubated for 20 min at 37 °C in a solution of 1% acetic acid and 50% EtOH to remove the dye. Finally, absorbance was measured at 540 nm using a microplate reader (Synergy-HT, BioTek).

ROS measurements

For the determination of ROS, HepG2 cells were exposed to 25 µg/mL QDs and NPs for approximately 24 h. Intracellular ROS production was measured using 2, 7-dichloro fluorescin diacetate (DCFH-DA) [43, 44], which can passively cross the cell membrane and react with ROS to produce a colored compound called dichlorofluorescein (DCF). Briefly, a 10 mM DCFH-DA stock solution was diluted in the culture medium, without other additives, to prepare a 100 µM working medium. After exposure to QDs and NPs, the cells were washed twice with HBS (HEPES buffered saline), and incubated with medium containing 100 µM DCFH-DA at 37 °C for 30 min. Intercellular fluorescence was analyzed using a fluorescence microscope (Olympus CKX 41; Olympus) at 20X magnification.

Measurement of mitochondrial membrane potential (MMP)

MMP was measured using the procedure described by Zhang et al. [45]. Briefly, HepG2 cells were exposed to 25 µg/mL QDs and NPs for 24 h. Subsequently, the cells were washed twice with PBS and treated with 10 µg/mL Rh 123, a fluorescent dye, for 1 h at 37 °C in the dark. The fluorescence of Rh 123 was measured using a fluorescence microscope (OLYMPUS CKX 41).

Glutathione level

For GSH measurement, HepG2 cells were cultured in 25 cm^2 culture flasks. The cells were exposed to 10, 25, and 50 µg/mL of (~6 ± 2 nm), (~15–20 nm), (~45–50 nm), and (~100 nm) Zn NPs for 24 h. Thereafter, the cells were lysed in cell lysis buffer [1 × 20 mM Tris–HCl (pH 7.5), 150 mM NaCl, 2.5 mM sodium pyrophosphate, 1 mM Na_2EDTA, and 1% Triton]. The supernatant, obtained after centrifugation at 15,000 × *g* for 10 min at 4 ºC, was kept on ice until assayed following Ellman's method [46]. Briefly, a mixture of 0.1 mL of cell extract (supernatant) and 0.9 mL of 5% TCA was centrifuged (2300 × *g* for 15 min at 4 °C). Thereafter, 0.5 mL of supernatant was added to 1.5 mL of 0.01% 5, 5-dithio-bis-(2-nitrobenzoic acid) (DTNB) and measured spectrophometrically at 412 nm.

Lipid peroxidation (LPO)

LPO was assayed by the method of Ohkawa et al. (1979) [47]. HepG2 cells were exposed to 10, 25, and 50 µg/mL of (~6 ± 2 nm), (~15–20 nm), (~45–50 nm), and (~100 nm) ZnO-NPs for 24 h. Briefly, 0.1 mL of cell extract and 1.9 mL of 0.1 M sodium phosphate buffer (pH 7.4) were incubated at 37 °C for 1 h. After incubation, cells were precipitated with 5% TCA and then centrifuged to 2300 × *g* for 15 min, to collect the supernatant. After incubation, 1.0 mL of 1% TBA was added to the supernatant and put in hot water for 15 min. After cooling, the absorbance was taken at 532 nm.

Analysis of cell-cycle progression by flow cytometry

Cell-cycle analysis was performed by a method described by Saquib et al. [48]. The cells were exposed to 50 µg/mL of ~6 ± 2 nm, ~15–20 nm, ~45–50 nm, and ~100 nm ZnO-NPs for 24 h and centrifuged at 1000 rpm for 4 min. The cells were fixed with 500 µL of 70% ice-cold ethanol, incubated at 4 °C for 1 h, washed with PBS, and stained using 500 µL of PBS, containing 50 µg of propidium iodide (PI)/mL, 0.1% Triton X-100, and 0.5 mg/mL RNAase. PI signal was measured by flow cytometry with a Beckman Coulter flow cytometer (Coulter Epics XL/Xl-MCL, USA) through a FL 3 filter (585 nm) and 10,000 events were acquired. The data were evaluated using Coulter Epics XL/ XL-MCL, System II Software, Version 3.0.

Quantitative real-time PCR analysis of apoptotic markers

HepG2 cells were cultured in 6-well plates and treated with ZnO QDs and NPs at a concentration of 50 µg/mL for 24 h. Total RNA was extracted both from treated and untreated cells by RNeasy mini Kit (Qiagen), as per the manufacturer's

instructions. RNA concentration was evaluated using Nanodrop 8000 spectrophotometer (Thermo-Scientific). cDNA was prepared from 1 µg of total RNA using M-MLV kit (Promega), as per the kit's protocol. Real-time quantitative PCR (RT-PCR) was done using Roche® LightCycler®480 (96-well block) (IN, USA), following the recommended cycling program. For the reaction mixture, 2 µL of cDNA was taken in a final volume of 20 µL of reaction mix. The RT-PCR program included a denaturation step at 95 °C for 10 min, followed by 40 cycles of denaturation at 95 °C for 15 s, annealing at 60 °C for 20 s, and elongation at 72 °C for 20 s. Expressed genes were normalized to GAPDH, the housekeeping control gene. All experiments were performed in triplicate and data were expressed as the mean of at least three experiments.

Results

Morphological analysis by FESEM

Morphological changes in the prepared QDs and NPs can be seen in the FESEM images (Fig. 1). Figure 1a, b shows FESEM images at lower and higher magnification, respectively, of the synthesized QDs and NPs, which confirmed that the synthesized ZnO products were of different sizes. The less magnified (Fig. 1a) image clearly demonstrated that the grown structures were high in density. Most QDs exhibited spherical shapes with an average diameter range of 6 ± 2 nm. Additionally, some QDs were ellipsoidal, as seen in the FESEM micrograph (Fig. 1b). The size of the NPs increased under different processing conditions, as described in Materials and methods. The NPs were elongated and triangular (Fig. 1c, d). The average size of each NP was in the range of ~ 15–20 nm (Fig. 1d). Upon annealing, NPs form aggregates or crystals. At high-temperature annealing (at 500 °C in air for 1 h), the powders resulted in random shapes of NPs, such as spherical, triangular, or circular, approximately 45–50 nm in size (Fig. 1e, f). A higher annealing temperature (< 500 °C) resulted in agglomeration of particles (~ 90–100 nm in size) to form bigger NPs, as shown in Fig. 1g, h. At higher temperature, small NPs merged with each other and in between other particles [19, 20, 25].

Morphological analysis by TEM

Further morphological investigation of QDs and NPs was performed with TEM. Figure 2a–d shows TEM images of particles grown to different sizes. The shapes were nearly spherical and were similar to those seen with FESEM (Fig. 1). As seen in the TEM image (Fig. 2a), the synthesized NPs were spherical and ellipsoidal in shape. The size of each QD was in the range of ~ 6 ± 2 nm, which was consistent with the FESEM data (Fig. 1b). In the second case, the size of NPs reached up to ~ 20 nm (Fig. 2b) and had similar morphology as depicted in the previous results (Fig. 1c, d). In the third case, the size of the NPs was seen to be up to ~ 45–50 nm (Fig. 2c) (at 500 °C for 1 h in air under ambient conditions) and the results were consistent with those from FESEM (Fig. 1e, g). At higher temperatures (above

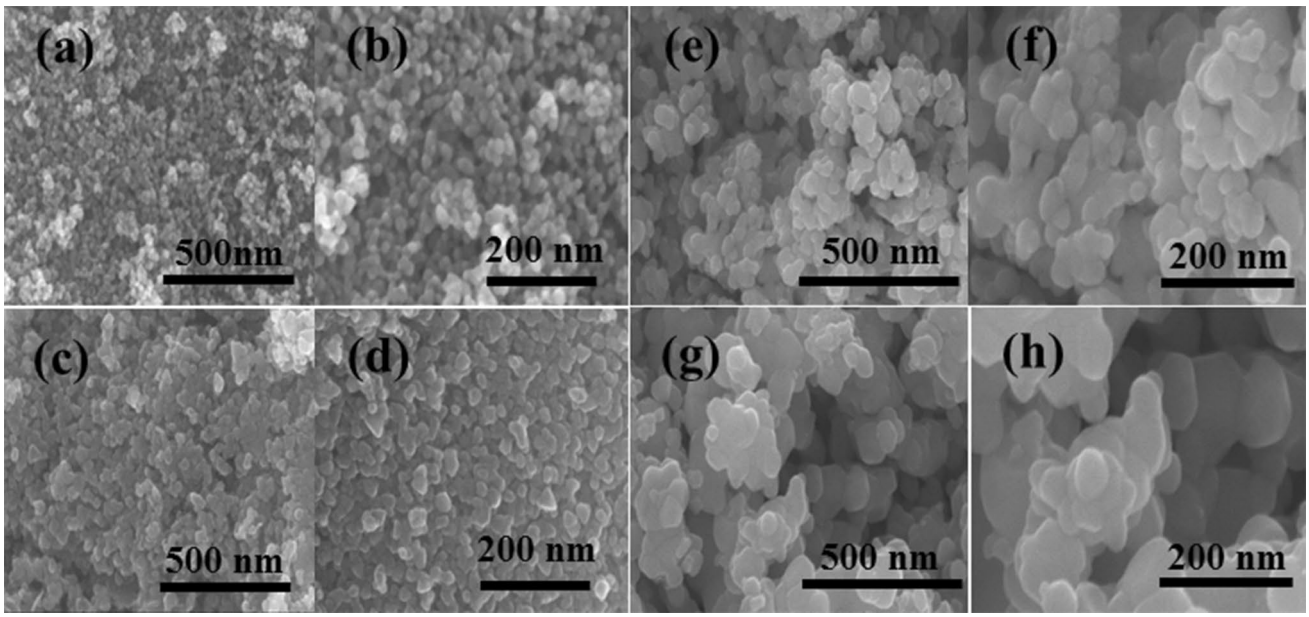

Fig. 1 Low and high magnified FESEM images of different sizes of ZnO QDs and NPs processed via solution process: **a**, **b** 6 ± 2 nm; **c**, **d** 15–20 nm; **e**, **f** ~ 45–50 nm and **g, h** ~ 100 nm

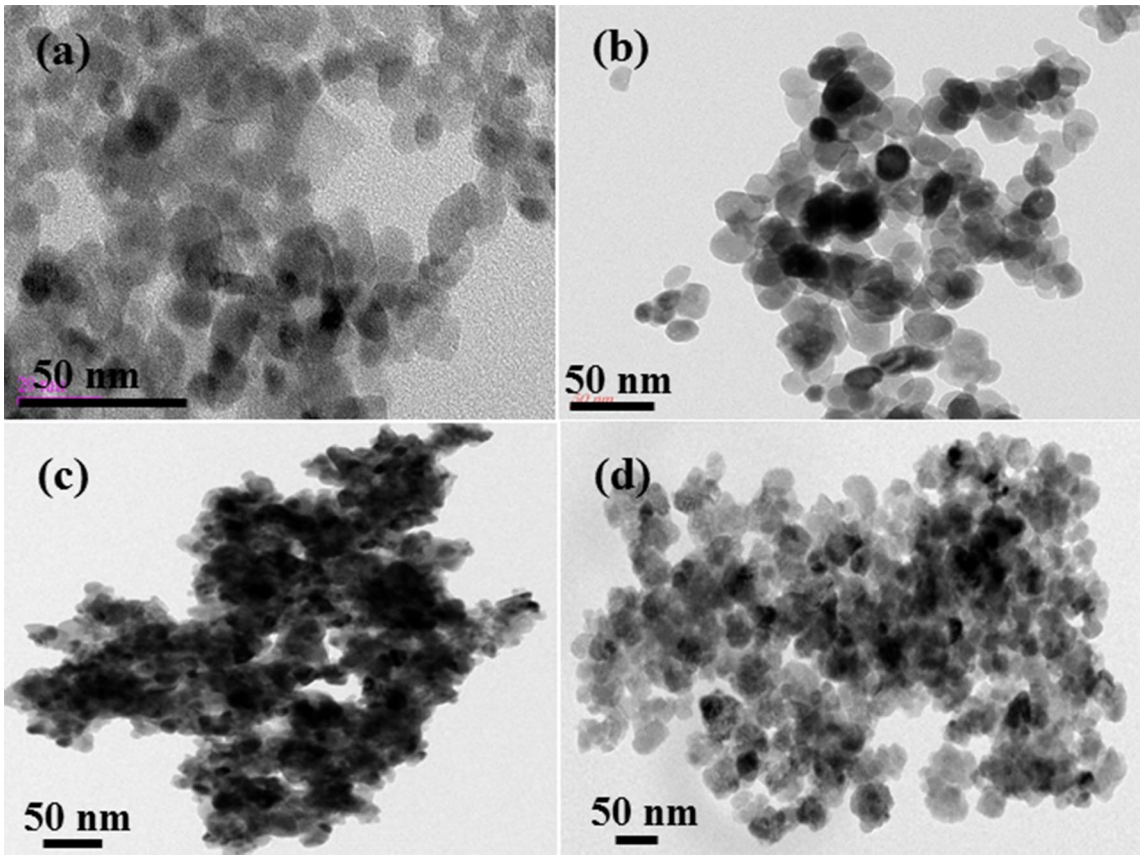

Fig. 2 TEM images of different sizes of QDs and NPs of ZnO prepared via solution process: **a, b** ~ 6 ± 2 nm; **c, d** ~ 15–20 nm; **e, f** ~ 45–50 nm and **g, h** ~ 100 nm

500 °C for 1 h), the NPs aggregated with each other and formed bigger sized structures (~ 90–100 nm) (Fig. 2d) [7, 19, 20, 25].

Crystallinity, phase and size examination (XRD results)

Figure S1 presents the X-ray diffraction patterns (XRD) of synthesized NPs at different processing conditions. The main indexed peaks <1010>, <0002>, <10 11> clearly showed the crystalline property of the nanoproducts. All indexed peaks in the spectrum obtained were well matched with bulk ZnO (JCPDS Card No. 36-1451), which further confirmed that the prepared powders were crystalline in nature and had wurtzite phase. There was no other peak related to impurities in the spectrum within the detection limit of the XRD, which again confirmed that the synthesized powders were pure ZnO [7, 19, 20, 25].

Cytotoxicity results

MTT and NRU results

The results of cytotoxicity assessment have been summarized in Figs. 3 and 4. HepG2 cells were treated with ZnO-NPs in concentrations ranging from 1–100 µg/mL for 24 h. The cytotoxicity of ZnO-NPs was observed by MTT and NRU assays. These assays showed that ZnO-NPs did not produce significant cytotoxicity at concentrations of 10 µg/mL and lower. However, at concentrations of 25 µg/mL and above, ZnO-NPs induced cytotoxicity in a concentration-dependent manner, resulting in the reduction of HepG2 cell viability. Furthermore, ZnO-NPs, approximately 15–20 nm in size, were most cytotoxic, followed by ZnO-NPs (~ 6 ± 2 nm) and ZnO-NPs (~ 45–50 nm). ZnO-NPs (~ 100 nm) were found to be least cytotoxic to HepG2 cells. Cell viability, using MTT assay, was recorded at 5%, 6%, and 54% in ZnO-NPs (~ 15–20 nm); 12%, 16%, and 90% in ZnO-NPs (~ 45–50 nm); 9%, 11%, and 20% in ZnO-QDs (~ 6 ± 2 nm); and 50%, 63%, and 63% at 25, 50, and 100 mg/mL ZnO concentration, respectively (Fig. 3).

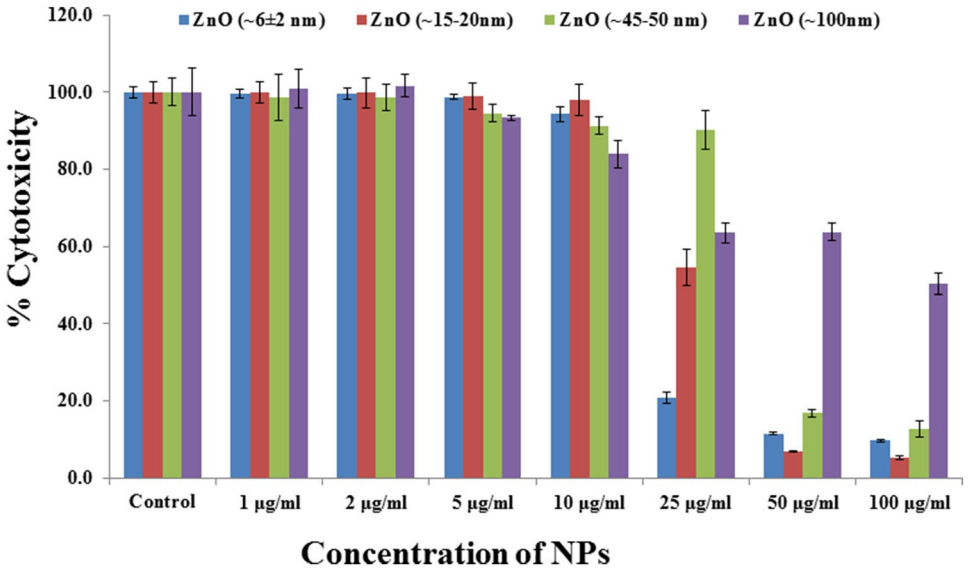

Fig. 3 Percent cell viability by MTT assay in HepG2 cells following exposure to various concentrations of ZnO nanoparticles: **a** ~ 6 ± 2 nm, **b** ~ 15–20 nm, **c** ~ 45–50 nm and **d** ~ 100 nm for 24 h. Values are mean ± SE of three independent experiments. *Statistically significant difference as compared to control ($p < 0.05$)

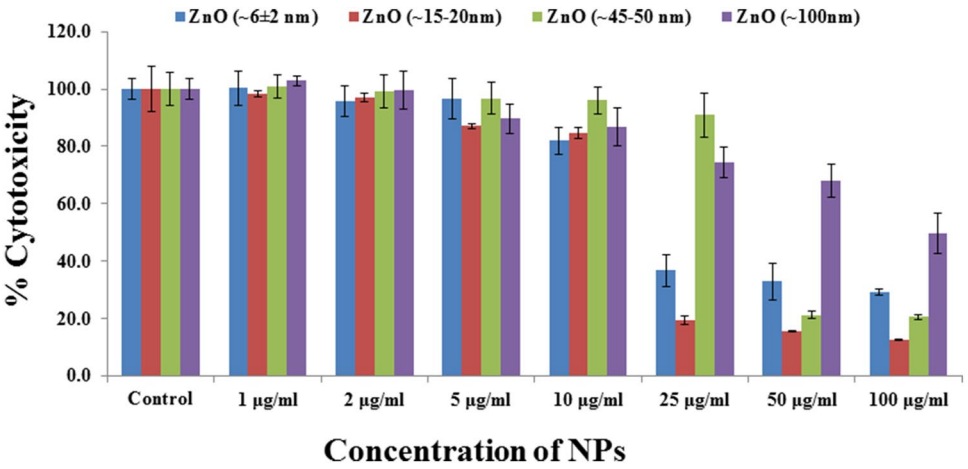

Fig. 4 Percent cell viability by NRU assay in HepG2 cells following the exposure of various concentrations of ZnO nanoparticles: **a** ~ 6 ± 2 nm, **b** ~ 15–20 nm, **c** ~ 45–50 nm and **d** ~ 100 nm for 24 h. Values are mean ± SE of three independent experiments. *Statistically significant difference as compared to control ($p < 0.05$)

As shown in Fig. 4, a similar trend of reduction in cell viability was recorded by the NRU assay. The cell viability by NRU assay was recorded as 12%, 15%, and 19% in ZnO-NPs (~ 15–20 nm); 20%, 21%, and 91% in ZnO-NPs (~ 45–50 nm); 29%, 32%, and 36% in ZnO-NPs (~ 6 ± 2 nm); and 49%, 68%, and 74% at 25, 50, and 100 µg/mL ZnO concentration, respectively (Fig. 4). The IC50 values obtained for (~ 6 ± 2 nm), (~ 15–20 nm), (~ 45–50 nm), and (~ 100 nm) ZnO-NPs were 15.8 µg/mL, 27.5 µg/mL, 30.08 µg/mL, and 101.2 µg/mL, respectively, by the MTT assay.

ZnO-NPs induced oxidative stress

ROS generation and GSH and LPO levels were examined to show the potential of ZnO-NPs to increase oxidative stress in HepG2 cells. The results revealed that HepG2 cells exposed to ZnO-NPs, had higher intracellular ROS generation (Fig. S2). Fluorescence microscopy results showed that ~ 6 ± 2 nm ZnO-QDs expressed more fluorescence intensity followed by ~ 15–20 nm, ~ 45–50 nm, and ~ 100 nm ZnO-NPs as compared to the untreated control (Fig. S2 graph). As shown in Fig. 5, the GSH level was considerably lower in HepG2 exposed to ZnO-NPs, however, the LPO level was higher (125, 148, and 174% was found in 6, 119, and 139 nm; 165% in 15–20, 110, and 122 nm; 147% in 50 nm and 100, 128, and 140% were found in 100 nm sized NPs, as compared with the control, which was 100% at different concentrations of NPs (10, 25, and 50 µg/mL), in HepG2 cells exposed to ZnO-NPs for 24 h (Fig. 6).

ZnO-NPs induced change in MMP level

MMP levels in HepG2 cells exposed to ZnO-NPs for 24 h at 25 µg/mL are presented in Fig. S3. The decrease in MMP levels was recorded in terms of fluorescence intensity of the mitochondria specific dye Rh 123. As shown in Fig. S3,

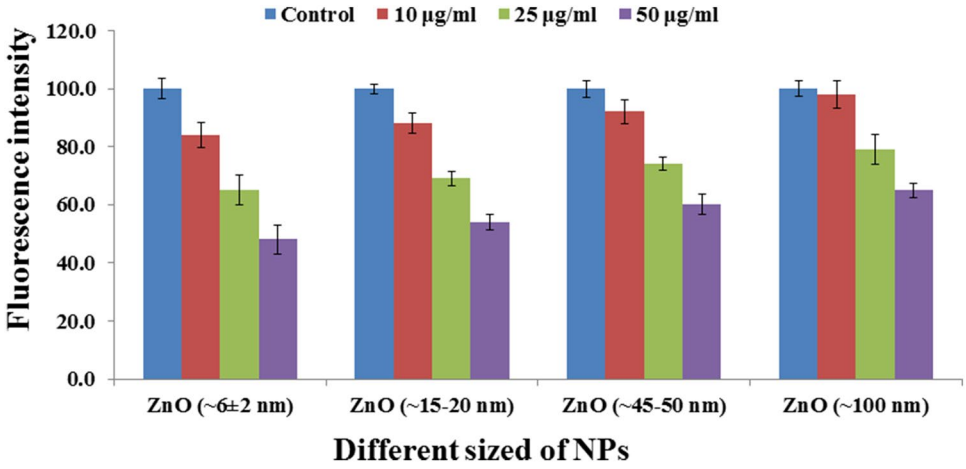

Fig. 5 Glutathione depletion in HepG2 cells exposed to various sizes of ZnO nanoparticles at different concentrations. Values are mean ± SE of three independent experiments. *Statistically significant difference as compared to control ($p < 0.05$)

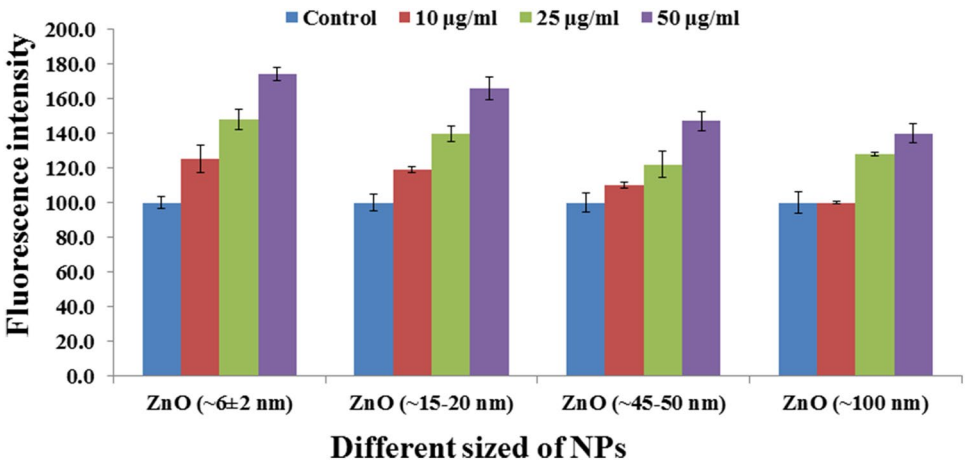

Fig. 6 Various sizes of ZnO nanoparticles induced lipid peroxidation in HepG2 cells exposed for 24 h at different concentrations. Values are mean ± SE of three independent experiments. *Statistically significant difference as compared to control ($p < 0.05$)

ZnO-NPs decreased the fluorescence intensity of Rh 123. This reduction in fluorescence intensity in HepG2 cells treated with ZnO-NPs indicated a significant decrease in MMP levels with low to high range of NPs (54, 45, 36, and 23) compared to the control (100).

Effect of different sized ZnO-NPs on cell-cycle progression

Analysis of the effects of varying sizes of zinc oxide NPs on HepG2 cells indicated an increase in the apoptotic sub-G_1 peak after 24 h of exposure (Fig. 7). With an average of 5.9% back ground level of apoptotic peaks in HepG2 control, ZnO-QDs (< 10 nm) at lower doses of 10 and 25 µg/mL did not show any changes in the normal cell cycle. At the higher concentration of 50 µg/mL, a significant increase of 24.4% in the sub-G_1 apoptotic phase was recorded (Fig. 7). HepG2 cells exposed to low doses of ZnO-NPs (< 20 nm) exhibited a typical pattern of G_2/M arrest. In comparison to 27.4% of the control cells in G_2/M phase, 10 and 25 µg/mL of ZnO-NPs (< 20 nm) treatment showed 42.4% and 33.1% cells in G_2/M phase, respectively. At the highest concentration of 50 µg/mL, ZnO-NPs (< 20 nm) exhibited transition of G_2/M arrested cells (16.5%) in the apoptotic phase (16.0%) (Fig. 7). A similar pattern of G_2/M arrest, along with an increase in apoptosis, was observed in ZnO-NPs-50 (< 50 nm)-treated HepG2 cells. Lower doses of 10 and 25 µg/mL exhibited 34.4% and 18.1% of cells arrested in G_2/M phase, respectively, vis-à-vis untreated control, which showed only 23.7% cells, in G_2/M phase. Nonetheless, bigger ZnO particles (~45–50 nm), at the highest concentration of 50 µg/mL, exhibited a substantial increase in apoptotic response with 27.2% cells in sub-G_1 phase, as compared to 8.8% of apoptotic cells in the untreated control group (Fig. 7). In comparison to treatment with larger sized ZnO nanoparticles, such as 100 nm, ~45–50 nm, and 15 ± 20 nm, HepG2 exposed to ZnO particles of 6 ± 2 nm, exhibited stronger apoptotic response during cell-cycle progression. Lower dose (10 and 25 µg/mL) exposure of HepG2 cells exhibited 16.4% and 22.8% increase in apoptotic sub-G_1 peak, respectively. At the highest concentration of 50 µg/mL, nearly 44% of cells underwent apoptosis (Fig. 7).

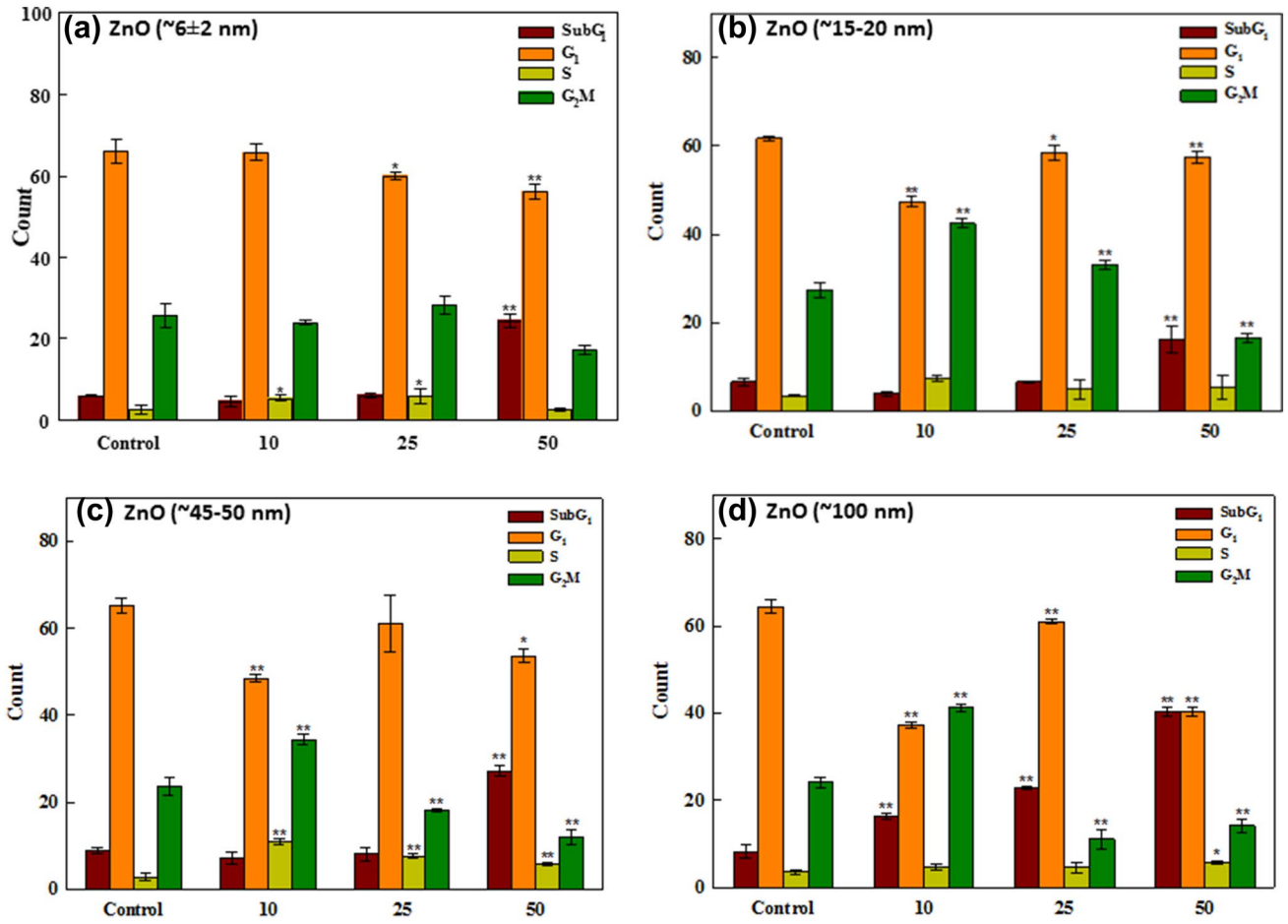

Fig. 7 Cell-cycle analysis of HepG2 cells exposed to ZnO nanoparticle of different sizes: **a** ~ 6 ± 2 nm size, **b** ~ 15–20 nm size, **c** ~ 45–50 nm size and **d** ~ 100 nm. Values are mean ± SE of three independent experiments. *Statistically significant difference compared to control ($p < 0.05$)

Analysis of mRNA level of apoptotic genes using quantitative real-time PCR

HepG2 cells were exposed to different sizes of ZnO-NPs for 24 h at a concentration of 50 µg/mL, and quantitative real-time PCR was performed to evaluate the mRNA level of apoptotic genes (p53, bax, casp3, and bcl-2). Different sized NPs significantly altered the regulation of apoptotic genes in HepG2 cells ($p < 0.05$ for each gene) (Fig. 8). The mRNA levels of the cell-cycle checkpoint or tumor suppressor gene p53 (Fig. 8) and the pro-apoptotic gene bax (Fig. 8) were upregulated. We also detected higher expression of the caspase-3(Fig. 8) gene in NP-treated cells. The expression of bcl-2 (Fig. 8), an anti-apoptotic gene, was downregulated in cells treated with different sized ZnO-NPs. Thus, ZnO-NPs of different sizes induced expression of apoptotic genes.

Discussion

QDs and NPs of ZnO have wide industrial and biomedical applications, such as in cancer, drug delivery, DNA damage, and cytotoxicity, due to their high surface area and catalytic properties [7, 19, 20, 25]. In this study, QDs and different sized NPs were prepared by soft chemical solution and annealing process using zinc acetate dihydrate with different reducing salts, such as octadecylamine and thiourea, at different processing parameters. The NP solutions were calibrated with acid (HCl) and base (NaOH) at desired concentrations [7, 19, 20, 25]. The QDs and NPs were characterized in terms of their crystalline and morphological properties with sophisticated instruments. Techniques such as XRD, FESEM, and TEM were used to check the crystallinity of the synthesized QDs and NPs. The FESEM and TEM results showed that the prepared nanostructures had diverse shapes, with a nearly smooth surface and an average diameter of 6–100 nm, for both QDs and NPs. High-resolution TEM (HR-TEM) confirmed that the structures had

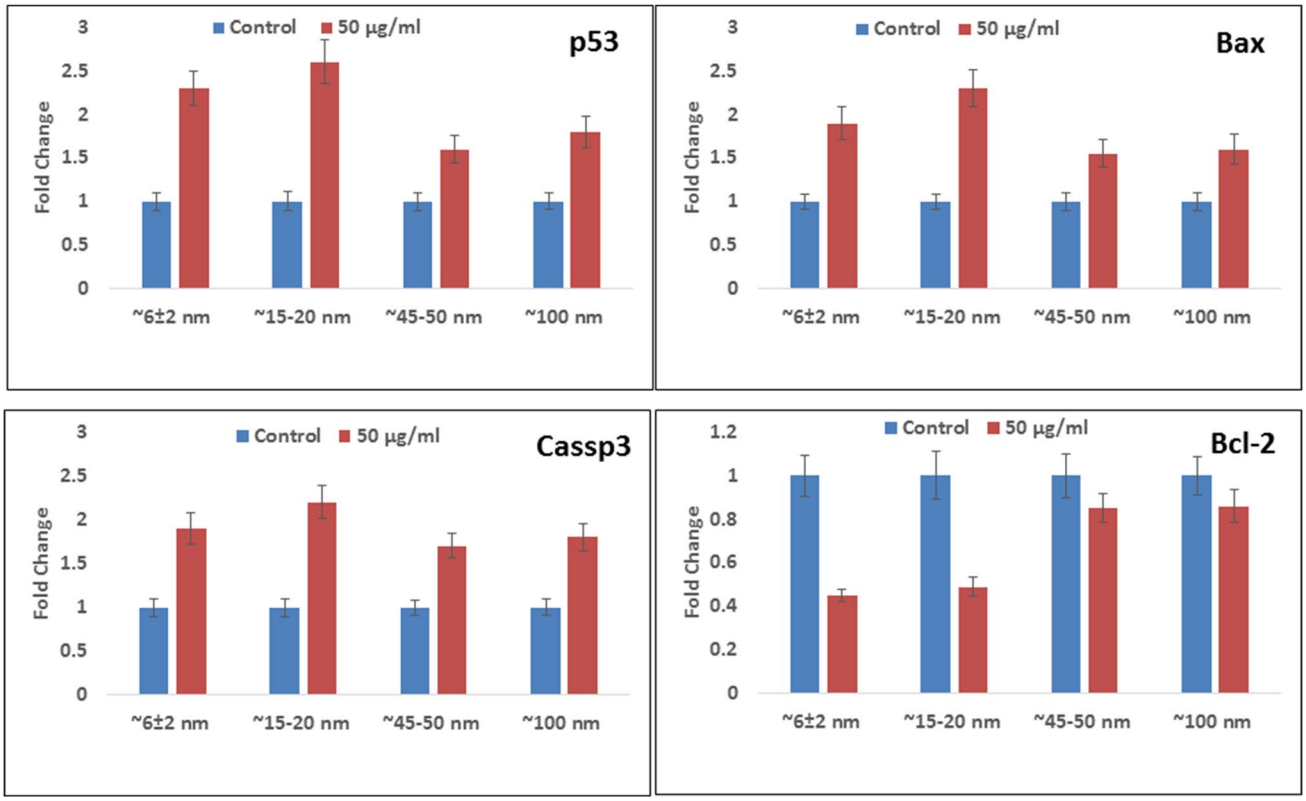

Fig. 8 For quantification of mRNA levels, fold change of apoptotic genes (p53, bax, and casp3) and anti-apoptotic gene (bcl-2) was analyzed. Cells were exposed to 50 µg/mL of different sized ZnO-NPs for 24 h. GAPDH was used as an internal control to normalize the data. The values are mean ± SE of three independent experiments. *Statistically significant difference as compared to control ($p < 0.05$)

lattice spacing (~ 0.256 nm), were crystalline, and equal to pure wurtzite phase ZnO [5]. The nanostructures of ZnO were optically active materials, which exhibited similar band gap to the commercial zinc oxide powder (3.37 eV) [5]. In addition to the detailed characterization of ZnO-NPs, the aim of this study was to also investigate the cytotoxic responses of different sized NPs on liver cancer (HepG2) cells. The MTT and NRU assays were used to check the cytotoxicity of different sized NPs on the cells after a 24-h incubation period. HepG2 cells exposed to 1–100 µg/mL doses of ZnO-NPs significantly decreased cell viability in a concentration-dependent manner. The results are in accordance with those published previously on cytotoxic activity of NPs, within the same range [49]. Cytotoxicity of these NPs on cancer cells is due to their morphological organization, and their characteristic differences and functions are responsible for cell death [50]. In addition to assessing the cytotoxicity of HepG2 cells caused by NPs and investigating its mechanism, we also evaluated ROS generation and mitochondrial membrane potential (MMP), which played a key role in the cytotoxicity of HepG2 exposed to ZnO-NPs for 24 h. ROS can disturb cellular function by acting directly on DNA, protein, and lipids, destroying their structure and leading to cell death [51]. In the present study, we showed that NPs induced ROS damage in a concentration-dependent manner in HepG2 cells. Our results are in agreement with those reported previously, where various types of NPs have been shown to induce ROS generation, oxidative stress, and cellular cytotoxicity [51–53]. Furthermore, we checked MMP levels in HepG2 cells exposed to differently shaped NPs, and observed that the NPs were responsible in decreasing the level of MMP, in terms of reduction in fluorescence intensity of Rh 123. The mitochondria is directly involved in apoptosis and a reduction in MMPs, which can trigger the release of apoptogenic factors from the mitochondria into the cytosol, leading to cell death [54, 55]. Thus, cell death was induced with interaction/exposure of different sized NPs resulting in an increase in ROS generation and a decrease in MMPs, when treated with ZnO-NPs.

To evaluate the size-dependent toxicity of ZnO-NPs, we studied cell death in HepG2 cells. A comparative analysis suggested that smaller sized ZnO particles (ZnO, ~ 6 ± 2 nm) directly induced apoptosis in HepG2 at the higher concentration of 50 µg/mL. Although ZnO particles of size ~ 15–20 and ~ 45–50 nm also induced apoptosis at a higher concentration of 50 µg/mL, a strong connection with G_2/M arrest was also revealed, indicating detrimental effects on DNA and cellular repair machinery. In contrast, we observed a

low dose-dependent augmentation of apoptosis in HepG2 cells, treated with smaller size QDs (ZnO, ~ 6 ± 2 nm). The appearance of sub-G_1 peak in cell-cycle analysis at increasing concentrations of ZnO-NPs suggested the possible involvement of early and late apoptotic/necrotic pathway genes, which might be triggered by alteration in mitochondrial and lysosomal functions [56, 57]. Moreover, HepG2 cells exhibited concentration-dependent G_2/M arrest with ZnO-NPs-20, ZnO-NPs-50, and ZnO-NPs-100, suggesting heavy DNA damage and failure of DNA repair machinery. Cellular DNA repair mechanisms are highly conserved [58], and extensive DNA damage may lead to cell-cycle arrest and cell death [59, 60]. Overall, our flow cytometry data clearly exhibited a size-based hierarchy of toxicity, where ZnO 100 > ZnO 50 > ZnO 20 > ZnO 6. Based on the physical (XRD, SEM, and TEM) and biological results (MTT and NRU assay, MMP levels, RT-PCR, and flow cytometry), we presented a schematic detail of the interaction of QDs/NPs with cells, production of ROS, and cells' death caused by nanostructures in a dose-dependent manner (Fig. 9).

Conclusion

In summary, we successfully synthesized different sized nanoparticles, such as QDs and NPs, using various chemical approaches under different conditions. The results from XRD showed that synthesized ZnO-NPs were pure and highly

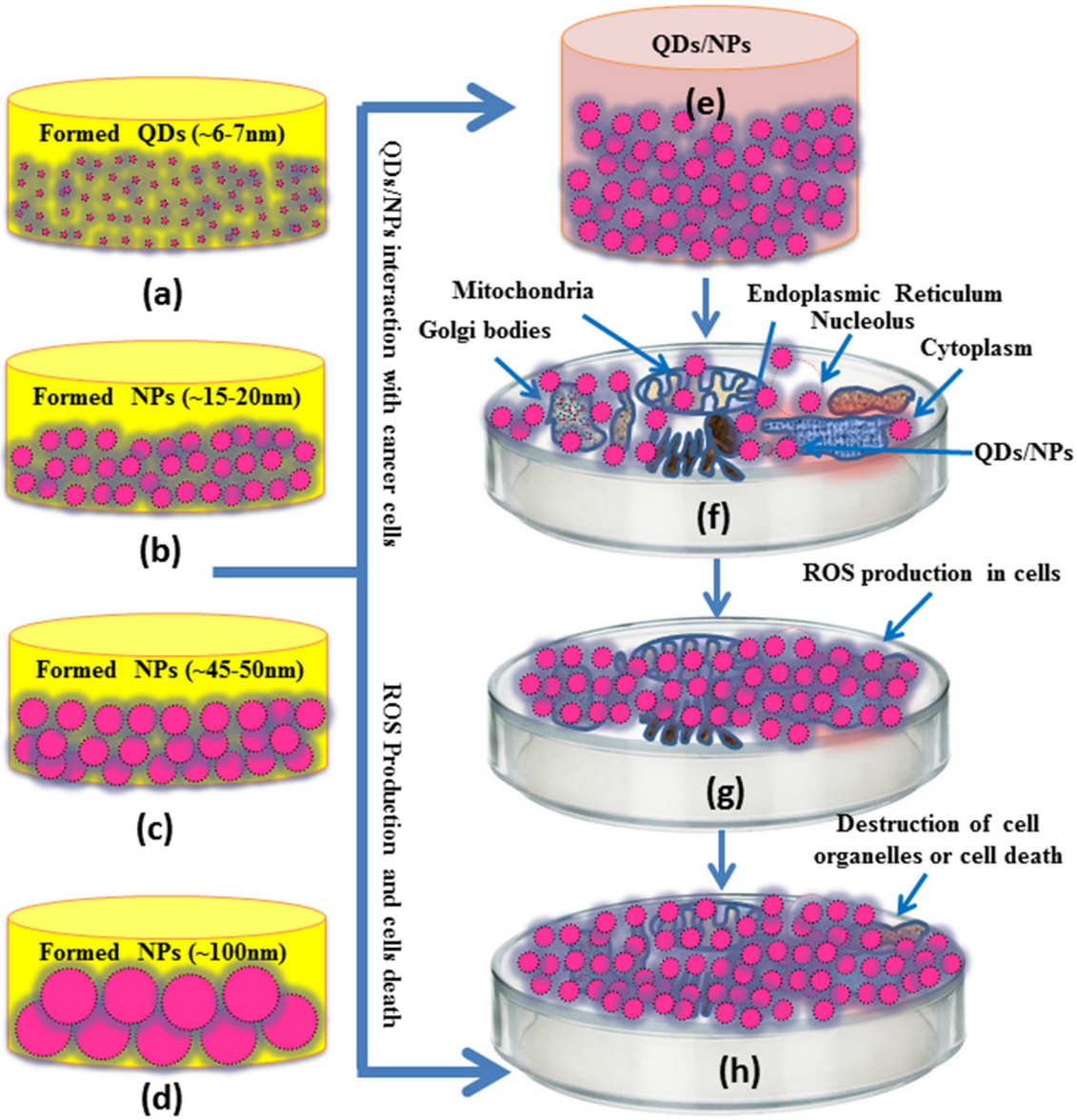

Fig. 9 Possible proposed schematic for the interaction of QDs and NPs with cells and subsequent cell death

crystalline in character. The morphological investigations revealed that the prepared structures retained a wurtzite hexagonal phase. In this context, the obtained FESEM images showed sequential data of QDs and NPs from 6 to 100 nm in spherical shape and was consistent with TEM observations. To characterize the prepared materials, different sized NPs were incubated with liver cancer cells (HEPG2). The viability of cells was measured via the MTT and NRU assays, which clearly showed that the small nanoparticles (QDs) were more potent as compared to the bigger sized NPs. The results showed that ~ 15–20 nm ZnO-NPs had high cytotoxicity, followed by ~ 6 ± 2 nm NPs, and ~ 45–50 nm NPs. Moreover, the larger NPs (~ 100 nm) were found to be less cytotoxic to HepG2 cells, which may be due to the settling of high-density NPs at the bottom of the culture medium, resulting in their reacting slowly with cancer cells. Similar observations were made with the NRU data, which showed that the reduction in cell viability was affected by the size of the NPs. Smaller particles could enter the cells easily, owing to low density, and damage intracellular organelles, whereas larger particles, with higher density, exhibited lower reactivity. Thus, cell death was influenced by the concentration and size of ZnO-NPs. In this context, ROS production in cells was examined and smaller (6 nm) particles were shown to express a higher intensity (166) in terms of % change in green fluorescence of DCF, as compared to particles of other sizes (152, 143, and 112) and untreated control (100). Additionally, the level of the antioxidant GSH was also considerably lower in HepG2 cells, incubated with different sized NPs—84, 65, and 48% was found in 6 nm; 88, 69, and 54% in 15–20 nm; 92, 74, and 60% in 50 nm and 98, 79, and 65% in 100 nm sized NPs, while the lipid peroxidation level was found to increase (125, 148, and 174% for 6 nm; 119, 139, and 165% for 15–20 nm; 110, 122, and 147% for 50 nm; and 100, 128, and 140% for 100 nm sized NPs, as compared to 100% for control, with different concentration of NPs) in HepG2 cells exposed to ZnO-NPs for 24 h. The reduction in MMP level in cancer cells with NPs again showed the significance of nanostructures. In addition, flow cytometry results showed that at the highest concentration of 50 μg/mL, almost 44% of cells had undergone apoptosis.

Several approaches, such as chemotherapy and radiotherapy, have been used for cancer treatment, but the results have been unsatisfactory. To date, the surgical procedure is very costly and tedious for the patients and the recovery is painful and time consuming. Extensive work is still needed to establish a successful therapy that might be able to cure cancer efficiently, effectively, and economically. Recent advances in nanotechnology have contributed in various areas of science and technology in cost-effective ways. The biological application of nanostructured materials could provide significant improvement to the existing technologies with no harmful side-effects due to their biocompatibility. Moreover, the small dimensions of NPs enable them to be delivered directly and quickly to cells and proteins as compared to other available drugs.

Acknowledgements The authors are grateful to the Deanship of Scientific Research, King Saud University for funding through Vice Deanship of Scientific Research Chairs.

Compliance with ethical standards

Conflicts of interest The authors declared that there is no conflicts of interest.

References

1. Chen RQ, Zou CW, Yan XD, Gao W (2011) Zinc oxide nanostructures and porous films produced by oxidation of zinc precursors in wet-oxygen atmosphere. Prog Nat Sci Mater Int 21:81–96
2. Ramimoghadam D, Hussein MZB, Taufiq-Yap YH (2013) Synthesis and characterization of ZnO nanostructures using palm olein as biotemplate. Chem Central J 7:71
3. Polarz S, Orlov AV, Schüth F, Lu AH (2007) Preparation of high-surface-area zinc oxide with ordered porosity, different pore sizes, and nanocrystalline walls. Chem Eur J 13:592–597
4. Wahab R, Ansari SG, Kim YS, Seo HK, Shin HS (2007) Room temperature synthesis of needle-shaped ZnO nanorods via sonochemical method. Appl Surf Sci 253:7622–7626
5. Wahab R, Ansari SG, Kim YS, Dar MA, Shin HS (2008) Synthesis and characterization of hydrozincite and its conversion into zinc oxide nanoparticles. J Alloy Compound 461:66–71
6. Wahab R, Khan F, Yang YB, Hwang IH, Shin HS, Ahmad J, Dwivedi S, Khan ST, Siddiqui MA, Saquib Q, Musarrat J, Al-Khedhairy AA, Mishra YK, Ali BA (2016) Zinc oxide quantum dots: multifunctional candidates for arresting C2C12 cancer cells and their role towards caspase 3 and 7 genes. RSC Adv 6:26111–26120
7. Ahmad J, Wahab R, Siddiqui MA, Musarrat J, Al-Khedhairy AA (2015) Zinc oxide quantum dots: a potential candidate to detain liver cancer cells. Bioproc Biosyst Eng 38:155–163
8. Neves MC, Trindade T, Timmons AMB, Jesus JDPD (2001) Synthetic hollow zinc oxide microparticles. Mater Res Bull 36:1099–1108
9. O'Brien S, Nolan MG, Çopuroglu M, Hamilton JA, Povey I, Pereira L, Martins R, Fortunato E, Pemble M (2010) Zinc oxide thin films: Characterization and potential applications. Thin Solid Films 518:4515–4519
10. Sathiya SM, Okram GS, Dhivya SM, Manivannan G, Rajan MAJ (2016) Interaction of chitosan/zinc oxide nanocomposites and their antibacterial activities with *Escherichia coli*. Mater Today 3:3855–3860
11. Hahm JI (2016) Fundamental properties of one-dimensional zinc oxide nanomaterials and implementations in various detection modes of enhanced biosensing. Annu Rev Phys Chem 67:691–717
12. Barankin MD, Gonzalez IIE, Ladwig AM, Hicks RF (2007) Plasma-enhanced chemical vapor deposition of zinc oxide at atmospheric pressure and low temperature. Sol Energ Mater Sol Cells 91:924–930
13. Filpo GD, Pantuso E, Armentano K, Formoso P, Profio GD, Poerio T, Fontananova E, Meringolo C, Mashin AI, Nicoletta FP (2018) Chemical vapor deposition of photo catalyst nanoparticles

on PVDF membranes for advanced oxidation processes. Membranes 8:35
14. Fouad OA, Ismail AA, Zaki ZI, Mohamed RM (2006) Zinc oxide thin films prepared by thermal evaporation deposition and its photocatalytic activity. Appl Catal B 62:144–149
15. Nian Q, Look D, Leedy K, Cheng GJ (2018) Optoelectronic performance enhance- ment in pulsed laser deposited gallium-doped zinc oxide (GZO) films after UV laser crystallization. Appl Phys A Mater Sci Process 2018:124. https://doi.org/10.1007/s00339-018-2032-4
16. Holmes J, Johnson K, Zhang B, Katz HE, Matthews JS (2012) Metal organic chemical vapor deposition of ZnO from β-ketoiminates. Appl Organomet Chem 26:267–272
17. Lee S, Umar A, Kim SH, Reddy NK, Hahn YB (2007) Growth of ZnO nanoneedles on silicon substrate by cyclic feeding chemical vapor deposition: Structural and optical properties. Korean J Chem Eng 24:1084–1088
18. Singh T, Pandya DK, Singh R (2011) Template assisted growth of zinc oxide based nanowires by electrochemical deposition. J Nano Electron Phys 3:146–150
19. Wahab R, Khan ST, Ahmad J, Musarrat J, Al-Khedhairy AA (2017) Functionalization of *anti-Brucella* antibody on ZnO-NPs and their deposition on aluminum sheet towards developing a sensor for the detection of *Brucella*. Vacuum 146:592–598
20. Wahab R, Ansari SG, Kim YS, Dhage MS, Seo HK, Song MW, Shin HS (2009) Effect of annealing on the conversion of ZnS to ZnO nanoparticles synthesized by the sol-gel method using zinc acetate and thiourea. Met Mater Int 15:453–458
21. Wahab R, Ansari SG, Seo HK, Kim YS, Suh EK, Shin HS (2009) Low temperature synthesis and characterization of rosette-like nanostructures of ZnO using solution process. Solid State Sci 11(2):439–443
22. Dev A, Panda SK, Kar S, Chakrabarti S, Chaudhuri S (2006) Surfactant-assisted route to synthesize well-aligned ZnO nanorod arrays on sol−gel-derived ZnO thin films. J Phys Chem B 110:14266–14272
23. Zhou Q, Xie B, Jin L, Chen W, Li J (2016) Hydrothermal synthesis and respon- sive characteristics of hierarchical zinc oxide nanoflowers to sulfur dioxide. J Nanotech. https://doi.org/10.1155/2016/6742104
24. Segovia M, Sotomayor C, Gonzalez G, Benavente E (2012) Zinc oxide nano structures by solvothermal synthesis. Mol Cryst Liq Cryst 555:40–50
25. Wahab R, Hwang IH, Kim YS, Musarrat J, Siddiqui MA, Seo HK, Tripathy SK, Shin HS (2011) Non-hydrolytic synthesis and photocatalytic studies of ZnO nanoparticles. Chem Eng J 175:450–457
26. Johnson JC, Yan H, Schaller RD, Petersen PB, Yang P, Saykally RJ (2002) Near-field imaging of nonlinear optical mixing in single zinc oxide nanowires. Nano Lett 2:279–283
27. Tyona MD, Osuji RU, Ezema FI (2013) A review of zinc oxide photoanode films for dye sensitized solar cells based on zinc oxide nanostructures. Adv Nano Res 1:43–58
28. Wahab R, Khan F, Ahmad N, Shin HS, Musarrat J, Al-Khedhairy AA (2013) Hydrogen adsorption properties of nano and microstructures of ZnO. J Nanomater. https://doi.org/10.1155/2013/542753
29. Wahab R, Kaushik NK, Verma AK, Mishra A, Hwang IH, Yang YB, Shin HS, Kim YS (2011) Fabrication and growth mechanism of ZnO nanostructures and their cytotoxic effect on human brain tumor U87, cervical cancer HeLa, and normal HEK cells. J Biol Inorg Chem 16:431–442
30. Wahab R, Khan F, Lutfullah SRB, Kaushik NK, Ahmad J, Siddiqui MA, Saquib Q, Ali BA, Khan ST, Musarrat J, Al-Khedhairy AA (2015) Utilization of photocatalytic ZnO nanoparticles for deactivation of safranine dye and their applications for statistical analysis. Phys E (Amsterd Neth) 69:101–108
31. Khan M, Naqvi AH, Ahmad M (2015) Comparative study of the cytotoxic and genotoxic potentials of zinc oxide and titanium dioxide nanoparticles. Toxicol Rep 2:765–774
32. Goh EG, Xu X, McCormick PG (2014) Effect of particle size on the UV absorbance of zinc oxide nanoparticles. SCR Mater 78–79:49–52
33. Hanley C, Thurber A, Hanna C, Punnoose A, Zhang J, Wingett DG (2009) The Influences of Cell Type and ZnO Nanoparticle Size on Immune Cell Cytotoxicity and Cytokine Induction. Nanoscale Res Lett 4:1409–1420
34. Najim N, Rusdi R, Hamzah AS, Shaameri Z, Zain MM, Kamarulzaman N (2014) Effects of the absorption behaviour of ZnO nanoparticles on cytotoxicity measurements. J Nanomater. https://doi.org/10.1155/2014/694737
35. Sahu D, Kannan GM, Tailang M, Vijayaraghavan R (2016) In vitro cytotoxicity of nanoparticles: a comparison between particle size and cell type. J Nanosci. https://doi.org/10.1155/2016/4023852
36. Li H, Yanan Z, Yang L, Linhua H, Huarong G (2017) Comparison of the in vitro and in vivo toxic effects of three sizes of zinc oxide (ZnO) particles using flounder gill (FG) cells and zebrafish embryos. J Ocean Univ China 16:93–106
37. Liu J, Kang Y, Yin S, Song B, Wei L, Chen L, Shao L (2017) Zinc oxide nano particles induce toxic responses in human neuroblastoma SHSY5Y cells in a size dependent manner. Inter J Nanomed 12:8085–8099
38. Sahu D, Kannan GM, Vijayaraghavan R (2014) Size dependent effect of zinc oxide on toxicity and inflammatory potential of human monocytes. J Toxicol Environ Health A 77:177–191
39. Wahab R, Mishra A, Yun SI, Kim YS, Shin HS (2010) Antibacterial activity of ZnO nanoparticles prepared via non-hydrolytic solution route. Appl Microbiol Biotechnol 87:1917–1925
40. Wahab R, Kim YS, Hwang IH, Shin HS (2009) A non-aqueous synthesis, characterization of zinc oxide nanoparticles and their interaction with DNA. Synth Metals 159:2443–2452
41. Wahab R, Ansari SG, Kim YS, Seo HK, Kim GS, Khang G, Shin HS (2007) Low temperature solution synthesis and characterization of ZnO nano-flowers. Mater Res Bull 42:1640–1648
42. Mosmann T (1983) Rapid colorimetric assay for cellular growth and survival: application to proliferation and cytotoxicity assays. J Immunol Methods 65:55–63
43. Borenfreund E, Puerner JA (1985) Toxicity determined in vitro by morphological alterations and neutral red absorption. Toxicol Lett 24:119–124
44. Siddiqui MA, Kashyap MP, Kumar V, Al-Khedhairy AA, Musarrat J, Pant AB (2010) Protective potential of trans-resveratrol against 4- hydroxy nonenal induced damage in PC12 cells. Toxicol In Vitro 24:1592–1598
45. Wróblewski F, Ladue JS (1955) Lactic dehydrogenase activity in blood. Proc Soc Exp Biol Med 90:210–213
46. Wang H, Joseph JA (1999) Quantifying cellular oxidative stress by dichlorofluorescein assay using microplate reader. Free Radic Biol Med 27:612–616
47. Zhang R, Pan X, Huang Z, Weber GF, Zhang G (2011) Osteopontin enhances the expression and activity of MMP-2 via the SDF-1/CXCR4 axis in hepatocellular carcinoma cell lines. PLoS One. https://doi.org/10.1371/journal.pone.0023831
48. Ellman GL (1959) Tissue sulphydryl groups. Arch Biochem Biophys 82:70–77
49. Ohkawa H, Ohishi N, Yagi K (1979) Assay for lipid peroxides in animal tissues by thiobarbituric acid reaction. Anal Biochem 95:351–358
50. Saquib Q, Al-Khedhairy AA, Ahmad J, Siddiqui MA, Dwivedi S, Khan ST, Musarrat J (2013) Zinc ferrite nanoparticles activate IL-1b, NFKB1, CCL21 and NOS2 signaling to induce mitochondrial dependent intrinsic apoptotic pathway in WISH cells. Toxicol Appl Pharmacol 273:289–297

51. Shen C, James SA, deJonge MD, Turney TW, Wright PF, Feltis BN (2013) Relating cytotoxicity, zinc ions, and reactive oxygen in ZnO nanoparticle exposed human immune cells. Toxicol Sci 136:120–130
52. Pujalté I, Passagne I, Brouillaud B, Tréguer M, Durand E, Ohayon-Courtès C, L'Azou B (2011) Cytotoxicity and oxidative stress induced by different metallic nanoparticles on human kidney cells. Part Fibre Toxicol 8:10
53. Khanna P, Ong C, Bay BH, Baeg GH (2015) Nanotoxicity: an interplay of oxidative stress, inflammation and cell death. Nanomaterials (Basel) 5:1163–1180
54. Li N, Sioutas C, Cho A, Misra C, Sempf J, Wang M, Oberley T, Froines J, Nel A (2003) Ultrafine particulate pollutants induce oxidative stress and mitochondrial damage. Env Health Perspect 111:455–460
55. Fu PP, Xia Q, Hwang HM, Ray PC, Yu H (2014) Mechanisms of nanotoxicity: generation of reactive oxygen species. J Food Drug Anal 22:64–75
56. Kroemer G, Galluzzi L, Brenner C (2007) Mitochondrial membrane permeabilization in cell death. Physiol Rev 87:99–163
57. Vandenabeele P, Galluzzi L, Berghe TV, Kroemer G (2010) Molecular mechanisms of necroptosis: an ordered cellular explosion. Nat Rev Mol Cell Biol 11:700–714
58. Nicoletti I, Migliorati G, Pagliacci MC, Grignani F, Riccardi C (1991) A rapid and simple method for measuring thymocyte apoptosis by propidium iodide staining and flow cytometry. J Immunol Methods 139:271–279
59. Ravi M, De SL, Azharuddin S, Pau SFD (2010) The beneficial effects of spirulina focusing on its immunomodulatory and antioxidant properties. Nutr Diet Suppl 2010:273–283
60. Ferreira CG, Epping M, Kruyt FA, Giaccone G (2002) Apoptosis: target of cancer therapy. Clin Cancer Res 8:2024–2034
61. Konopa J (1988) G2 block induced by DNA crosslinking agents and its possible consequence. Biochem Pharmacol 37:2303–2309
62. Tsao YP, Arpa PD, Liu LF (1992) The involvement of active DNA synthesis in camptothecin-induced G2 arrest: altered regulation of p34cdc2/cyclin B. Cancer Res 52:1823–1829

Affiliations

Javed Ahmad[1,2] · Rizwan Wahab[1,2] · Maqsood A. Siddiqui[1,2] · Quaiser Saquib[1,2] · Abdulaziz A. Al-Khedhairy[1]

✉ Javed Ahmad
javedbiochem@gmail.com

✉ Rizwan Wahab
rwahab05@gmail.com

[1] Zoology Department, College of Sciences, King Saud University, Riyadh 11451, Saudi Arabia

[2] Al-Jeraisy, Chair for DNA Research, King Saud University, Riyadh 11451, Saudi Arabia